ELSEVIER

Contents lists available at ScienceDirect

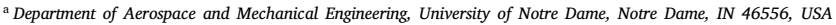
## International Journal of Non-Linear Mechanics

journal homepage: www.elsevier.com/locate/nlm



## Surface pressure reduces stability in bilayered systems under compression

Mohsen Darayi a, Maria A. Holland a,b,\*



<sup>&</sup>lt;sup>b</sup> Bioengineering Graduate Program, University of Notre Dame, Notre Dame, IN 46556, USA



## ARTICLE INFO

Keywords:
Buckling
Instability
Film-substrate system
Surface pressure
Neo-Hookean
Uniform compression

#### ABSTRACT

Buckling instabilities of layered materials are an important phenomenon that has been analyzed both analytically and numerically, but generally only in the absence of surface pressure. In this study, we present a linear stability analysis of the wrinkling of an inhomogeneous bilayer made up of dissimilar neo-Hookean elastic materials, under uniaxial compression with pressure applied to the top surface. Using a variational method, we investigate the effects of stiffness ratio and pressure boundary condition on buckling instabilities. In all cases, the addition of surface pressure decreases the stability of the system to some extent. For softer films, the pressure is the dominant influence on the instability of the system. In stiffer films, however, pressure loading and stiffness ratio interact to affect the unstable state of the bilayer system. Our results indicate that for a sufficiently high value of stiffness ratio  $\mu_{\rm f}/\mu_{\rm s} \gtrsim 10$ , the instability of the system does not depend on pressure.

### 1. Introduction

The understanding of wrinkling and buckling behaviors of layered materials is essential in various biological and engineering systems, with examples ranging from brain development [1,2] to stretchable electronics [3,4] and multilayer composites [5,6]. Under axial compression, layered materials transition from a stable equilibrium to an unstable state when the compressive load reaches a critical value. These instabilities have been investigated since the middle of the 20th century [7]. Researchers have since then identified how instabilities depend on physical and mechanical properties such as layer thickness, layer stiffness, and material anisotropy [8–10].

Wrinkling instabilities have been analyzed extensively for several different layered structures, particularly bilayers consisting of a thin film attached to a thicker substrate with different material properties. The wrinkling behavior of a material depends on the loading condition [11], which could result from uniform compression of both materials [12,13] or pre-stretch [14,15], growth [16,17], swelling [18, 19], or shrinking [20,21] in either of the two materials.

There has been much work on characterizing the critical strains and wavelengths of bilayers with zero stress boundary conditions at the free surface [22–24], but less is understood about the effects of external pressure on the onset of buckling. This is relevant, however, as layered systems are sometimes subjected to a boundary condition of constant or variable pressure, such as water pressure on the earth's crust at ocean depths or wind pressure on structures. Pressure boundary conditions are also common in the brain and other biological systems. Here, we

focus on the brain as a model system for a soft bilayered material under pressure. We build on the large body of work modeling the developing brain as a soft bilayer under planar compression [1,2,25]. At a macroscopic level, the brain consists of a thin outer layer of gray matter (cortex) adhered to a larger volume of white matter (subcortex) (Fig. 1). Although there is some disagreement in the literature, mechanical characterization studies on the brain tissue have calculated that the stiffness of white matter is 0.5 kPa to 2 kPa and gray matter 0.5 kPa to 3 kPa [26]. The outer cortical layer is surrounded by cerebrospinal fluid (CSF), which exerts a pressure ranging from 0.2 kPa in infants to 6 kPa in severe cases [27,28]. Studies have shown that the average normal CSF pressure in adults is approximately 2 kPa, with high and low CSF pressures in adults often associated with neurological disorders [29,30].

Previous studies have investigated the stability of spherical and cylindrical multilayers with the presence of external/internal pressure [31–40]. However, despite results demonstrating the influence of pressure on instabilities, only limited research exists regarding the role of non-zero stress boundaries on the instabilities of a bilayer made of a thin flat film bound to a thick substrate. One recent paper [41] briefly looked at the instabilities of a rectangular bilayer with normal pressure acting on the top surface of the film, but based on their plane-strain analysis they concluded that the pressure does not affect wrinkling instabilities. However, previous work has emphasized the effect of mechanical constraints on cortical folding patterns [42]. Thus, here we are interested in determining whether the cerebrospinal fluid pressure affects cortical instabilities.

<sup>\*</sup> Corresponding author at: Department of Aerospace and Mechanical Engineering, University of Notre Dame, Notre Dame, IN 46556, USA. E-mail address: maria-holland@nd.edu (M.A. Holland).

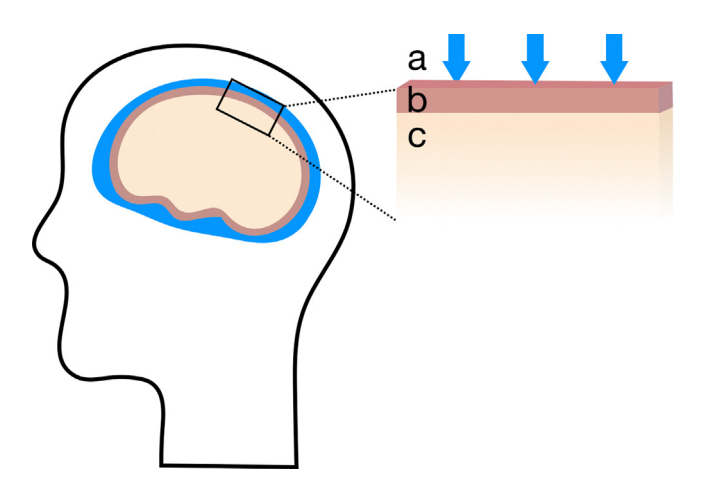


**Fig. 1.** Schematic of the human brain *in situ* (left) and as modeled here (right). Our model contains (a) cerebrospinal fluid, (b) gray matter, and (c) white matter.

In this study, we consider the case of an inhomogeneous bilayer under compression with pressure applied to the top surface. The film and the substrate are both incompressible neo-Hookean material with shear modulus  $\mu_{\rm f}$  and  $\mu_{\rm s}$ , respectively. The bilayer undergoes a uniform compression followed by an imposed wrinkling perturbation, where we determine what amount of compression makes the buckled state energetically favorable. We seek buckling instabilities to analyze the effects of non-zero stress boundary conditions. Additionally, we discuss the impacts of the stiffness ratio between film and substrate on the buckling of the system.

## 2. Homogeneous deformation

In this section, we present an energy stability analysis to investigate the response of a bilayer system that undergoes a homogeneous deformation under an applied axial compression of  $\lambda_1 < 1$  along with applied in-plane and surface pressures. The coordinates of the material points are denoted as **X** in the undeformed reference configuration  $\Omega_0$  surrounded by its boundary  $\partial\Omega_0$  (Fig. 2). The coordinates in the resulting uniformly-compressed state are defined by **x**. Throughout this study, this uniformly compressed state is referred to as the intermediate configuration  $\Omega_i$  with its boundary denoted by  $\partial\Omega_i$ . The displacement vector field connecting the reference and intermediate configuration is  $\mathbf{U} = \mathbf{x} - \mathbf{X}$ , where the coordinates of the material points are related by  $x_i = \lambda_i X_i$  (i = 1,2,3). Accordingly, the deformation gradient of this homogeneous compression is  $\mathbf{F}_0 = \mathbf{I} + \partial \mathbf{U}/\partial\mathbf{X}$ , where  $\mathbf{I}$  is the second-order identity tensor. The deformation gradient in matrix form is

$$\mathbf{F}_0 = \begin{bmatrix} U_{1,1} + 1 & 0 & 0 \\ 0 & U_{2,2} + 1 & 0 \\ 0 & 0 & U_{3,3} + 1 \end{bmatrix}. \tag{2.1}$$

The film and substrate are assumed to be incompressible neo-Hookean hyperelastic materials. We allow for the possibility that the shear moduli of the film and the substrate are different,  $\mu_{\rm f} \neq \mu_{\rm s}$ , enabling our model to account for bilayer systems with a range of mechanical properties. The strain energy density per unit reference volume of the system is defined as

$$\Psi_0 = \frac{\mu}{2} \left[ \operatorname{tr}(\mathbf{C}_0) - \operatorname{tr}(\mathbf{I}) \right], \tag{2.2}$$

expressed in terms of the right Cauchy–Green deformation tensor  $\mathbf{C}_0 = \mathbf{F}_0^T \mathbf{F}_0$  and its trace  $\mathrm{tr}(\mathbf{C}_0) = [U_{1,1}+1]^2 + [U_{2,2}+1]^2 + [U_{3,3}+1]^2$ .

We consider a pressure loading condition on the boundary of the reference domain,  $\partial\Omega_0$ , where traction vectors  $\mathbf{T}_2$ ,  $\mathbf{T}_3^f$ , and  $\mathbf{T}_3^s$  are imposed on the top and front faces of the cuboid bilayer system (with the superscripts and representing film and substrate, respectively).

The traction is defined as  $\mathbf{T}=\mathbf{P}\cdot\mathbf{N}$ , where  $\mathbf{P}$  is the first Piola–Kirchhoff stress tensor and  $\mathbf{N}=[N_1,N_2,N_3]^T$  is the outward unit normal to the surface in the reference configuration. We assume that the pressures are constant, so the First Piola–Kirchhoff stress applied to the top surface is  $\mathbf{P}_2=-P_2\mathbf{e}_2\otimes\mathbf{e}_2$ , and in-plane stresses from adjacent material in the film and substrate are  $\mathbf{P}_3^f=-P_3^f\mathbf{e}_3\otimes\mathbf{e}_3$  and  $\mathbf{P}_3^s=-P_3^s\mathbf{e}_3\otimes\mathbf{e}_3$ , respectively. Thus, the Piola–Kirchhoff tractions can be written as  $\mathbf{T}_2=-P_2\,\mathbf{e}_2$ ,  $\mathbf{T}_3^f=-P_3^f\,\mathbf{e}_3$ , and  $\mathbf{T}_3^s=-P_3^s\,\mathbf{e}_3$ . The total free energy functional  $\Pi$  of both strain energy density and loads is thus

$$\Pi(\mathbf{U}, P_0) = \int_{\Omega_0} \mu_m \left[ \frac{1}{2} \left[ \text{tr}(\mathbf{C}_0) - \text{tr}(\mathbf{I}) \right] - P_0[J_0 - 1] \right] dV - \int_{\partial \Omega_0} \mathbf{T} \cdot \mathbf{U} dS,$$
(2.3)

where  $P_0$  is the hydrostatic pressure acting as the Lagrange multiplier to enforce the incompressibility condition,  $J_0$  is the determinant of  $F_0$ , and m = f, s for the film and the substrate, respectively.

Substitution of the obtained relations into Eq. (2.3) leads to

$$\begin{split} \Pi(\mathbf{U},P_0) &= \int_{\varOmega_0} \mu_m \left[ \frac{1}{2} \left[ [U_{1,1} + 1]^2 + [U_{2,2} + 1]^2 + [U_{3,3} + 1]^2 - 3 \right] \right. \\ &\left. - P_0 \left[ [U_{1,1} + 1][U_{2,2} + 1][U_{3,3} + 1] - 1 \right] \right] \mathrm{d}V \\ &+ \int_{\partial\varOmega_{0,\mathrm{top}}} P_2 U_2 N_2 \mathrm{d}S + \int_{\partial\varOmega_{0,\mathrm{front}}} P_3^f U_3 N_3 \mathrm{d}S \\ &+ \int_{\partial\varOmega_{0,\mathrm{front}}} P_3^s U_3 N_3 \mathrm{d}S \,. \end{split} \tag{2.4}$$

We take the first variation of the functional with respect to displacement field **U** and the Lagrange multiplier  $P_0$ , and integrate by parts to remove the partial derivatives on the variations. Given that the displacement field is  $\mathbf{U} = X_1[\lambda_1 - 1]\mathbf{e}_1 + X_2[\lambda_2 - 1]\mathbf{e}_2 + X_3[\lambda_3 - 1]\mathbf{e}_3$ ,  $U_{i,ii} = 0$ , (i = 1, 2, 3). The stationary position of the energy functional is obtained when the first variation of the energy functional vanishes,

$$\begin{split} 0 &\doteq \delta \Pi(\mathbf{U}, P_0) = \int_{\varOmega_0} \mu_m \Big[ [U_{1,1} + 1][U_{2,2} + 1][U_{3,3} + 1] - 1 \Big] \delta P_0 \mathrm{d}V \\ &+ \int_{\partial\varOmega_{0,\mathrm{top}}} \Big[ \mu_\mathrm{f} [U_{2,2} + 1] - \mu_\mathrm{f} P_0 [U_{1,1} + 1][U_{3,3} + 1] + P_2 \Big] \\ &\times N_2 \delta U_2 \mathrm{d}S \\ &+ \int_{\partial\varOmega_{0,\mathrm{front}}} \Big[ \mu_\mathrm{f} [U_{3,3} + 1] - \mu_\mathrm{f} P_0 [U_{1,1} + 1][U_{2,2} + 1] + P_3^\mathrm{f} \Big] \\ &\times N_3 \delta U_3 \mathrm{d}S \\ &+ \int_{\partial\varOmega_{0,\mathrm{front}}} \Big[ \mu_\mathrm{s} [U_{3,3} + 1] - \mu_\mathrm{s} P_0 [U_{1,1} + 1][U_{2,2} + 1] + P_3^\mathrm{s} \Big] \\ &\times N_3 \delta U_3 \mathrm{d}S \,. \end{split}$$

Minimization of the potential energy functional over variations in  $P_0$  gives the constraint of incompressibility,

$$[U_{1,1} + 1][U_{2,2} + 1][U_{3,3} + 1] = \lambda_1 \lambda_2 \lambda_3 = 1.$$
(2.6)

Minimizing the energy with respect to variations in  $\boldsymbol{U}$  leads to the following set of boundary condition equations:

$$0 = \mu_{\rm f} \lambda_2 - \mu_{\rm f} \lambda_1 \lambda_3 P_0 + P_2 ,$$

$$0 = \mu_{\rm f} \lambda_3 - \mu_{\rm f} \lambda_1 \lambda_2 P_0 + P_3^{\rm f} ,$$
and 
$$0 = \mu_{\rm s} \lambda_3 - \mu_{\rm s} \lambda_1 \lambda_2 P_0 + P_3^{\rm s} .$$
(2.7)

These equations, using Eq. (2.6), yield the following results:

$$0 = \lambda_3^2 + \frac{P_3^f}{\mu_f} \lambda_3 - \frac{1}{\lambda_1^2 \lambda_3^2} - \frac{1}{\lambda_1 \lambda_3} \frac{P_2}{\mu_f} \quad \text{and} \quad P_3^f = \beta P_3^s,$$
 (2.8)

where we introduce the stiffness ratio  $\beta$  as the ratio of the shear moduli of the film and surface,  $\beta = \mu_{\rm f}/\mu_{\rm s}$ . We use the Newton–Raphson method to solve Eq. (2.8) for the exact value of transverse stretch  $\lambda_3$  that will result from the applied pressures  $P_2$  and  $P_3^{\rm f}$ , axial stretch  $\lambda_1$ , and the stiffness ratio  $\beta$ .

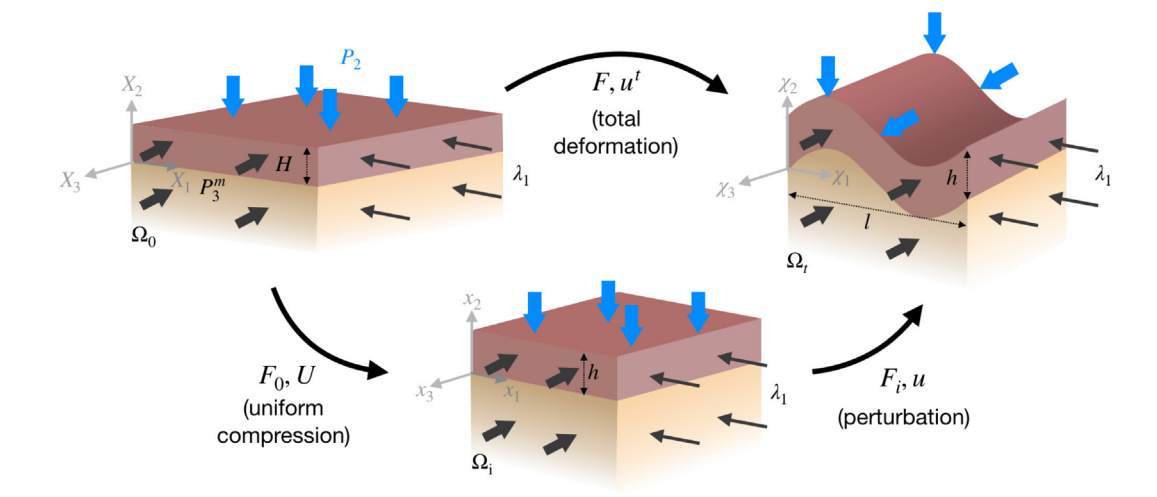


Fig. 2. Kinematics of bilayer instabilities, relating the system of a film on an infinite-sized substrate in  $\Omega_0$ , the reference configuration;  $\Omega_l$ , the intermediate configuration under homogeneous compression; and  $\Omega_l$ , the deformed configuration with wrinkles of wavelength l and wave number k.

#### 3. Perturbation deformation

Here we apply a linear stability analysis to find the buckling instabilities of our bilayer system. Now the homogeneous compression is followed by an imposed sinusoidal wrinkling deformation, transforming the intermediate configuration,  $\Omega_i$ , into the deformed configuration,  $\Omega_i$ . The displacement of particles in the body is  $\mathbf{u}(x_1, x_2) = \chi - \mathbf{x}$ , with  $\chi$  and  $\mathbf{x}$  representing the coordinates in the deformed and intermediate configurations, respectively. The total displacement of a material point from the reference configuration to the final deformed configuration is

$$\mathbf{u}^{t}(\mathbf{X}) = \mathbf{U}(\mathbf{X}) + \mathbf{u}(\mathbf{X}) = \mathbf{x}(\mathbf{X}) - \mathbf{X} + \mathbf{u}(\mathbf{X}),$$
 (3.1)

where  $\mathbf{u}(\mathbf{X}) = \mathbf{u}(\lambda_1 X_1, \lambda_2 X_2)$ . Therefore, the total deformation gradient will be

$$\mathbf{F} = \mathbf{I} + \frac{\partial \mathbf{u}^{t}}{\partial \mathbf{X}} = \mathbf{I} + \frac{\partial \mathbf{U}}{\partial \mathbf{X}} + \frac{\partial \mathbf{u}}{\partial \mathbf{X}}$$

$$= \begin{bmatrix} \lambda_{1} + \partial u_{1}/\partial X_{1} & \partial u_{1}/\partial X_{2} & 0\\ \partial u_{2}/\partial X_{1} & \lambda_{2} + \partial u_{2}/\partial X_{2} & 0\\ 0 & 0 & \lambda_{2} \end{bmatrix}. \tag{3.2}$$

The total potential energy of the system is given by a functional over the unit reference volume.

$$H(\mathbf{u}^{\mathbf{t}}, p) = \int_{\Omega_{0}} \mu_{m} \left[ \frac{1}{2} [\operatorname{tr}(\mathbf{C}) - 3] - p[\operatorname{det}(\mathbf{F}) - 1] \right] dV - \int_{\partial \Omega_{0}} \mathbf{T} \cdot \mathbf{u}^{\mathbf{t}} dS, \quad (3.3)$$

where  $\mathbf{C} = \mathbf{F}^T\mathbf{F}$  is the total right Cauchy–Green deformation tensor and  $p(\lambda_1X_1,\lambda_2X_2) = \mu_m[P_0 + P^m(\lambda_1X_1,\lambda_2X_2)]$  is the Lagrange multiplier to enforce the constraint of incompressibility, with  $\mu_mP_0$  representing the pressure in the uniformly compressed state and  $\mu_mP^m(\lambda_1X_1,\lambda_2X_2)$  (written as a function of coordinates in the reference configuration) corresponding to the pressure required to maintain a constant volume in the final configuration [11] and m=f,s for the film and the substrate, respectively.

In order to obtain all variables in the intermediate configuration, we perform a change of variables,

$$dV = dv/J_0, \quad \text{where } J_0 = 1$$

$$\frac{\partial u_i}{\partial X_J} = \frac{\partial u_i}{\partial x_k} \frac{\partial x_k}{\partial X_J} = \frac{\partial u_i}{\partial x_k} \mathbf{F}_{0,kJ}.$$
(3.4)

Because the pressure is a configuration-dependent load, meaning that the direction of the force remains normal to the top surface during the deformation but the magnitude of the force is the same in all the configurations [43], the following relation holds:

$$force = \mathbf{T} \cdot d\mathbf{S} = \mathbf{t} \cdot d\mathbf{s}, \tag{3.5}$$

where **t** is the Cauchy traction in the intermediate configuration, and ds is the surface in the intermediate configuration. The Cauchy traction vector can be written in terms of the first Piola–Kirchhoff stress as

$$\mathbf{t} = \boldsymbol{\sigma} \cdot \mathbf{n} = J_0^{-1} \mathbf{P} \mathbf{F}_0^T \cdot \mathbf{n}, \tag{3.6}$$

where  $\mathbf{n} = [n_1, n_2, n_3]$  is the unit normal to the surface in the intermediate configuration. By substituting Eqs. (3.4) and (3.6) into Eq. (3.3), the total potential energy of the bilayer system can be written in terms of the quantities defined in the intermediate configuration as

$$\begin{split} \Pi(\mathbf{u}^{m},P^{m}) &= \int_{\varOmega} \mu_{m} \left[ \begin{array}{c} \frac{1}{2} \left[ \left[ u_{1,1}^{m^{2}} + 2u_{1,1}^{m} + u_{2,1}^{m^{2}} + 1 \right] \lambda_{1}^{2} \right. \right. \\ & \left. + \left[ u_{1,2}^{m} + u_{2,2}^{m^{2}} + 2u_{2,2}^{m} + 1 \right] / \lambda_{1}^{2} \lambda_{3}^{2} + \lambda_{3}^{2} - 3 \right] \\ & \left. - P_{0} \left[ u_{1,1}^{m} + u_{2,2}^{m} + u_{1,1}^{m} u_{2,2}^{m} - u_{2,1}^{m} u_{1,2}^{m} \right] \right. \\ & \left. - P^{m} \left[ u_{1,1}^{m} + u_{2,2}^{m} + u_{1,1}^{m} u_{2,2}^{m} - u_{2,1}^{m} u_{1,2}^{m} \right] \right. \\ & \left. + P_{2} \lambda_{2} u_{2,2}^{m} - P_{2} + P_{2} \lambda_{2} \right] dv \\ & \left. + \int_{\delta \varOmega_{\text{front}}^{f}} P_{3}^{f} \lambda_{3} \left[ u_{3}^{f} + U_{3}^{f} \right] ds + \int_{\delta \varOmega_{\text{front}}^{s}} P_{3}^{s} \lambda_{3} \left[ u_{3}^{s} + U_{3}^{s} \right] ds \,, \end{split}$$

where  $u_1$  and  $u_2$  are periodic functions along the  $x_1$  and  $x_2$  axes with  $u_3=0$  (Fig. 2), and  $u_{i,j}$  denotes the derivative of the imposed wrinkling displacement in the ith direction with respect to  $\mathbf{x}_j$ , the coordinates in the intermediate configuration. Knowing that u is a periodic function,  $\int_v u_{i,i} \, \mathrm{d}v = 0$  for i=1,2,3. Following previous works [8,11,44,45], we only consider the quadratic terms. We compute the first variation of the functional with respect to  $u_1(\mathbf{x})$ ,  $u_2(\mathbf{x})$ , and  $P(\mathbf{x})$  and integrate by parts to find the stationary condition,

$$\begin{split} 0 &\doteq \delta \Pi(\mathbf{u}^m, P^m) = \int_{\Omega_i} \mu_m \left[ \left[ \lambda_1^2 u_{1,11}^m - P_{,1}^m + \frac{u_{1,22}^m}{\lambda_1^2 \lambda_3^2} \right] \delta u_1^m \right. \\ & + \left[ \frac{u_{2,22}^m}{\lambda_1^2 \lambda_3^2} - P_{,2}^m + \lambda_1^2 u_{2,11}^m \right] \delta u_2^m \\ & - \left[ u_{1,1}^m + u_{2,2}^m \right] \delta P^m \right] \mathrm{d}v \\ & - \int_{\delta \Omega_i} \mu_m \left[ \left[ \left[ \lambda_1^2 u_{1,1}^m - P_0 u_{2,2}^m - P^m \right] n_1 \right. \right. \\ & + \left[ \frac{u_{1,2}^m}{\lambda_1^2 \lambda_3^2} + P_0 u_{2,1}^m \right] n_2 \right] \delta u_1^m \\ & + \left[ \left[ \frac{u_{2,2}^m}{\lambda_1^2 \lambda_3^2} - P_0 u_{1,1}^m - P^m \right] n_2 \right] \end{split}$$

+ 
$$\left[\lambda_1^2 u_{2,1}^m + P_0 u_{1,2}\right] n_1 \delta u_2^m ds$$
. (3.8)

The Euler-Lagrange equations are obtained when each volume integral is set equal to zero:

$$0 = \lambda_1^2 u_{1,11}^m + \frac{u_{1,22}^m}{\lambda_1^2 \lambda_3^2} - P_{,1}^m, \tag{3.9}$$

$$0 = \frac{u_{2,22}^m}{\lambda_1^2 \lambda_2^2} + \lambda_1^2 u_{2,11}^m - P_{,2}^m, \tag{3.10}$$

and 
$$0 = u_{1,1}^m + u_{2,2}^m$$
. (3.11)

We assume that both film and substrate are adhered to each other, with traction and displacement continuity existing across the interface, located at the origin (see Fig. 2). As the substrate is modeled as infinitely thick, the displacements at the bottom  $(x_2 = -\infty)$  must vanish. Thus, the boundary conditions are given as

$$u_i^s = u_i^f = u_i$$
 at  $x_2 = 0$  and  $0 = u_i^s$  at  $x_2 = -\infty$   
for  $i = 1, 2$ . (3.12)

The surface integrals in Eq. (3.8) must also vanish, yielding the natural boundary equations,

$$0 = \frac{u_{1,2}^{f}}{\lambda_{1}^{2}\lambda_{3}^{2}} + P_{0}u_{2,1}^{f} \quad \text{at} \quad x_{2} = h$$

$$0 = \frac{u_{2,2}^{f}}{\lambda_{1}^{2}\lambda_{3}^{2}} + P_{0}u_{2,2}^{f} - P^{f} \quad \text{at} \quad x_{2} = h$$

$$0 = \beta \left[ \frac{u_{1,2}^{f}}{\lambda_{1}^{2}\lambda_{3}^{2}} + P_{0}u_{2,1}^{f} \right] - \left[ \frac{u_{1,2}^{s}}{\lambda_{1}^{2}\lambda_{3}^{2}} + P_{0}u_{2,1}^{s} \right] \quad \text{at} \quad x_{2} = 0$$

$$0 = \beta \left[ \frac{u_{2,2}^{f}}{\lambda_{1}^{2}\lambda_{3}^{2}} + P_{0}u_{2,2}^{f} - P^{f} \right] - \left[ \frac{u_{2,2}^{s}}{\lambda_{1}^{2}\lambda_{3}^{2}} + P_{0}u_{2,2}^{s} - P^{s} \right] \quad \text{at} \quad x_{2} = 0.$$

$$(3.13)$$

## 4. Linear perturbation analysis

We seek the unstable state of the bilayer using a linear stability analysis for a wrinkling pattern of the form

$$u_1^m(x_1, x_2) = f_1^m(x_2) \sin(kx_1)$$

$$u_2^m(x_1, x_2) = f_2^m(x_2) \cos(kx_1)$$

$$P^m(x_1, x_2) = f_3^m(x_2) \cos(kx_1),$$
(4.1)

where  $f_1^m$ ,  $f_2^m$ , and  $f_3^m$  are three unknown functions, k is the wave number in the intermediate configuration, and  $l=2\pi/k$  is the wavelength in the intermediate configuration. These quantities are related to their reference counterparts (Fig. 2) by

$$h = HF_{0,22} = \frac{H}{\lambda_1 \lambda_3}$$
 and  $k = \frac{K}{F_{0,11}} = \frac{K}{\lambda_1}$ . (4.2)

Substituting Eq. (4.1) into the Euler–Lagrange equations (Eqs. (3.9)–(3.11)) yields an ordinary differential equation with respect to  $f_1^m$ ,  $f_2^m$ , and  $f_3^m$ , with solution [45]:

$$\begin{split} u_1^m(x_1,x_2) &= \left[ c_1^m e^{-kx_2} - c_2^m e^{kx_2} + c_3^m \lambda_1^2 \lambda_3 e^{-k\lambda_1^2 \lambda_3 x_2} - c_4^m \lambda_1^2 \lambda_3 e^{k\lambda_1^2 \lambda_3 x_2} \right] \\ &\times \sin(kx_1) \,, \\ u_2^m(x_1,x_2) &= \left[ c_1^m e^{-kx_2} + c_2^m e^{kx_2} + c_3^m e^{-k\lambda_1^2 \lambda_3 x_2} + c_4^m e^{k\lambda_1^2 \lambda_3 x_2} \right] \cos(kx_1) \,, \\ P^m(x_1,x_2) &= \left[ \lambda_1^2 - \frac{1}{\lambda_1^2 \lambda_3^2} \right] \left[ c_1^m k e^{-kx_2} - c_2^m k e^{kx_2} \right] \cos(kx_1) \,, \end{split} \tag{4.3}$$

where  $c_i^m$  (m = f, s) are coefficients to be determined from the essential and natural boundary conditions. From the essential boundary condition on the bottom, Eq. ((3.12)b),

$$0 = u_1^{s}(x_1, -\infty) = u_2^{s}(x_1, -\infty) \longrightarrow c_1^{s} = 0, c_3^{s} = 0,$$
(4.4)

and from the condition of displacement continuity, Eq. ((3.12)a),

$$u_1^s(x_1,0) = u_1^f(x_1,0) \longrightarrow 0 = -c_1^f + c_2^f - c_3^f \lambda_1^2 \lambda_3 + c_4^f \lambda_1^2 \lambda_3 - c_2^s - c_4^s \lambda_1^2 \lambda_3,$$
(4.5)

$$u_2^{s}(x_1, 0) = u_2^{f}(x_1, 0) \longrightarrow 0 = c_1^{f} + c_2^{f} + c_3^{f} + c_4^{f} - c_2^{s} - c_4^{s}$$
 (4.6)

Substituting Eq. (4.3) into the four natural boundary equations, Eq. (3.13), we obtain four linear algebraic equations:

$$\begin{split} 0 &= \frac{1}{\lambda_{1}^{2}\lambda_{3}^{2}} \left[ -c_{1}^{f}e^{-kh} - c_{2}^{f}e^{kh} - c_{3}^{f}\lambda_{1}^{4}\lambda_{3}^{2}e^{-k\lambda_{1}^{2}\lambda_{3}h} - c_{4}^{f}\lambda_{1}^{4}\lambda_{3}^{2}e^{k\lambda_{1}^{2}\lambda_{3}h} \right] \\ &- P_{0} \left[ c_{1}^{f}e^{-kh} + c_{2}^{f}e^{kh} + c_{3}^{f}e^{-k\lambda_{1}^{2}\lambda_{3}h} + c_{4}^{f}e^{k\lambda_{1}^{2}\lambda_{3}h} \right] \\ 0 &= \left[ \frac{1}{\lambda_{1}^{2}\lambda_{3}^{2}} + P_{0} \right] \left[ -c_{1}^{f}e^{-kh} + c_{2}^{f}e^{kh} - c_{3}^{f}\lambda_{1}^{2}\lambda_{3}e^{-k\lambda_{1}^{2}\lambda_{3}h} + c_{4}^{f}\lambda_{1}^{2}\lambda_{3}e^{k\lambda_{1}^{2}\lambda_{3}h} \right] \\ &- \left[ \lambda_{1}^{2} - \frac{1}{\lambda_{1}^{2}\lambda_{3}^{2}} \right] \left[ c_{1}^{f}e^{-kh} - c_{2}^{f}e^{kh} \right] \\ 0 &= \beta \frac{1}{\lambda_{1}^{2}\lambda_{3}^{2}} \left[ -c_{1}^{f} - c_{2}^{f} - c_{3}^{f}\lambda_{1}^{4}\lambda_{3}^{2} - c_{4}^{f}\lambda_{1}^{4}\lambda_{3}^{2} \right] - \beta P_{0} \left[ c_{1}^{f} + c_{2}^{f} + c_{3}^{f} + c_{4}^{f} \right] \\ &- \left[ \frac{1}{\lambda_{1}^{2}\lambda_{3}^{2}} \right] \left[ -c_{2}^{s} - c_{3}^{s}\lambda_{1}^{4}\lambda_{3}^{2} - c_{4}^{f}\lambda_{1}^{4}\lambda_{3}^{2} \right] - \beta P_{0} \left[ c_{1}^{f} + c_{2}^{f} + c_{3}^{f} + c_{4}^{f} \right] \\ 0 &= \beta \left[ \frac{1}{\lambda_{1}^{2}\lambda_{3}^{2}} + P_{0} \right] \left[ -c_{1}^{f} + c_{2}^{f} - c_{3}^{f}\lambda_{1}^{2}\lambda_{3} + c_{4}^{f}\lambda_{1}^{2}\lambda_{3} \right] - \beta \left[ \lambda_{1}^{2} - \frac{1}{\lambda_{1}^{2}\lambda_{3}^{2}} \right] \left[ c_{1}^{f} - c_{2}^{f} \right] \\ &- \left[ \frac{1}{\lambda_{1}^{2}\lambda_{3}^{2}} + P_{0} \right] \left[ c_{2}^{s} + c_{3}^{s}\lambda_{1}^{2}\lambda_{3} + c_{4}^{f}\lambda_{1}^{2}\lambda_{3} \right] - \beta \left[ \lambda_{1}^{2} - \frac{1}{\lambda_{1}^{2}\lambda_{3}^{2}} \right] \left[ c_{1}^{f} - c_{2}^{f} \right] \\ &- \left[ \frac{1}{\lambda_{1}^{2}\lambda_{3}^{2}} + P_{0} \right] \left[ c_{2}^{s} + c_{3}^{s}\lambda_{1}^{2}\lambda_{3} + c_{4}^{f}\lambda_{1}^{2}\lambda_{3} \right] - \beta \left[ \lambda_{1}^{2} - \frac{1}{\lambda_{1}^{2}\lambda_{3}^{2}} \right] \left[ c_{1}^{f} - c_{2}^{f} \right] \end{aligned}$$

The essential and natural boundary conditions from Eqs. (4.5)–(4.10) form a set of six equations with six unknown constants  $c_i^m$  (i = 1, 2, 3, 4; m = s, f, where  $c_1^s = 0$  and  $c_3^s = 0$ ). To examine the stability of the bilayer, we solve this system of equation numerically. The corresponding system of equations has a form of

$$\mathbf{M} \left[ c_1^{f}, c_2^{f}, c_2^{f}, c_3^{f}, c_3^{s}, c_4^{s} \right]^T = 0 \tag{4.11}$$

where **M** is a 6 × 6 matrix given in Box I. The stationary of the potential energy is where a non-trivial solution for this system exists, or  $\det(\mathbf{M}) = 0$ . Utilizing Ridder's bracketing method [46], we numerically solve Eq. (4.11) for various axial and in-plane stretches ( $\lambda_1$ ,  $\lambda_3$ ) and shear moduli ratios ( $\beta$ ) to consider the effects of stiffness ratio and applied external pressure on wrinkling. The resulting critical strains resulting from the eigenvalue problem are the unstable points of our system, and the threshold critical values are the minimum critical strain and its corresponding wavelength.

Note that the effect of surface and transverse pressures  $(P_2, P_3^f)$ , and  $P_3^s)$  is accounted for in the value of transverse stretch that results from the prescribed loading. Eq. (2.8) shows that the in-plane pressure exerted on the film  $P_3^f$  and the substrate  $P_3^s$  are related by stiffness ratio  $\beta$ ; thus we only use the applied pressures to the film's surfaces  $(P_2, P_3^f)$  to analyze the buckling behavior of the system, normalizing them both by the shear modulus of the film  $\mu_f$ .

## 5. Results and discussion

As one motivating factor for our study is to determine the effects of CSF pressure on cortical folding, we focus on systems where the shear moduli of the two materials are similar,  $0.1 < \beta < 4$ . Considering the range of gray matter shear modulus (0.5 kPa to 3 kPa) and physiological CSF pressure (0.2 kPa to 2 kPa), the normalized pressure  $P_2/\mu_{\rm f}$  is chosen between 0.1 and 4. We further assume that the in-plane pressure,  $P_3^{\rm f}$ , is proportional to the pressure applied to the top surface,  $P_3^{\rm f} = 1.3 P_2$ .

## 5.1. Effect of pressure on transverse stretch

Here, we show that the surface and in-plane pressures naturally lead to changes in the transverse stretch based on Eq. (2.8) (Fig. 3).

$$\mathbf{M} = \begin{bmatrix} -1 & 1 & \lambda_1^2 \lambda_3 & \lambda_1^2 \lambda_3 & -1 & -\lambda_1^2 \lambda_3 \\ 1 & 1 & 1 & 1 & -1 & -1 \\ \left[\frac{1}{\lambda_1^2 \lambda_3^2} + P_0\right] e^{-\frac{KH}{\lambda_1^2 \lambda_3}} & \left[\frac{1}{\lambda_1^2 \lambda_3^2} + P_0\right] e^{\frac{KH}{\lambda_1^2 \lambda_3}} & \left[\lambda_1^2 + P_0\right] e^{-KH} & \left[\lambda_1^2 + P_0\right] e^{KH} & 0 & 0 \\ -\left[P_0 + \lambda_1^2\right] e^{-\frac{KH}{\lambda_1^2 \lambda_3}} & \left[P_0 + \lambda_1^2\right] e^{\frac{KH}{\lambda_1^2 \lambda_3}} & -\left[\frac{1}{\lambda_1^2 \lambda_3^2} + P_0\right] \lambda_1^2 \lambda_3 e^{-KH} & \left[\frac{1}{\lambda_1^2 \lambda_3^2} + P_0\right] \lambda_1^2 \lambda_3 e^{KH} & 0 & 0 \\ \beta \left[\frac{1}{\lambda_1^2 \lambda_3^2} + P_0\right] & \beta \left[\frac{1}{\lambda_1^2 \lambda_3^2} + P_0\right] & \beta \left[\lambda_1^2 + P_0\right] & \beta \left[\lambda_1^2 + P_0\right] & -\frac{1}{\lambda_1^2 \lambda_3^2} - P_0 & -\lambda_1^2 - P_0 \\ \beta \left[P_0 + \lambda_1^2\right] & -\beta \left[P_0 + \lambda_1^2\right] & \beta \left[\frac{1}{\lambda_3} + P_0 \lambda_1^2 \lambda_3\right] & -\beta \left[\frac{1}{\lambda_3} + P_0 \lambda_1^2 \lambda_3\right] & P_0 + \lambda_1^2 & \frac{1}{\lambda_3} + P_0 \lambda_1^2 \lambda_3 \end{bmatrix}$$

Box I.

This behavior arises because applying surface pressure to the bilayer under uniaxial compression will change the stretch in the thickness direction and require compensating changes in the transverse stretch. We consider a combination of values for  $P_2$  and  $P_3^{\rm f}$ , including cases where  $P_2 > P_3^{\rm f}$  ( $P_3^{\rm f} = 0$  and  $P_3^{\rm f} = 0.8P_2$  in Fig. 3, top row) and cases in which  $P_2 < P_3^{\rm f}$  ( $P_3^{\rm f} = 1.3P_2$  and  $P_3^{\rm f} = 2P_2$  in Fig. 3, bottom row). Resulting transverse stretches are compared with a bilayer under uniaxial compression with no applied surface pressure.

For a given value of axial stretch  $\lambda_1$ , when the surface pressure dominates (Fig. 3, top) the transverse stretch increases as the surface pressure increases, and when the transverse pressure dominates (Fig. 3, bottom) increasing the surface pressure decreases the transverse stretch. In both cases, the transverse stretch resulting from a pressure loading boundary deviates from the transverse stretch of a bilayer with zero-stress boundary condition subjected to compression. This analysis indicates that deformation should be expected to exhibit changes depending on pressure loading boundary conditions.

## 5.2. The relative influence of stiffness ratio and pressure on the stability of the bilayer

To investigate the effects of stiffness ratio and pressure at the top surface on a film-substrate system, we analyzed the threshold critical strain for 1600 combination of stiffness ratio and normalized surface pressure (Fig. 4). We consider four regions in Fig. 4 with distinct behaviors. In region A, the film is softer than the substrate and under low pressure (Fig. 6a). In this regime, the stiffness ratio has almost no effect on the stability of the system, but the stability decreases as the normalized pressure increase from 0 to 2. Region B represents the stiffer film regime with low applied pressure (Fig. 6b). Here, the stability decreases as  $\beta$  increases. Furthermore, while increases in pressure still decrease the stability, the pressure has less of an effect as the film becomes stiffer. In region C, where the film is softer and under higher pressures, the stiffness ratio maintains its dominance, with the maximum stability of the system being found as  $\beta \rightarrow 0$  (Fig. 7). In region D, with stiff films under higher pressures, the instability of the system is dominated by the stiffness ratio when the stiffness contrast between the film and the substrate are very low, while pressure dominates at moderate stiffness ratios (Fig. 4, far right). Finally, we note that discontinuities in the threshold critical strain occur at the boundary between regions B and D, and in region C, which will be discussed later.

## 5.3. Bilayer with stress-free vs. non-zero stress boundary condition

We reproduced the results of our previous study [11] for the case of a bilayer with a stress-free boundary condition under both plane strain  $(\lambda_3 = 1)$  and uniaxial compression  $(\lambda_3 = 1/\sqrt{\lambda_1})$ . We compared these results with our system of a 3D bilayer under uniaxial compression

with the addition of a pressure boundary condition (Fig. 5). The threshold values illustrate that the pressure boundary condition affects the stability of a film/substrate system by decreasing the threshold strain for the onset of instability. The results demonstrate that the system under uniform compression with pressure applied to the top surface is more unstable than the same system without pressure, under both plane strain compression (Fig. 5a) and uniaxial compression (Fig. 5b). The effect of pressure is more significant on systems with stiffer films  $(\beta > 1)$  than on systems with softer films  $(\beta > 1)$ .

### 5.3.1. Influence of stiffness ratio on stability in the presence of pressure

In order to examine the influence of stiffness ratio on the stability, we hold the pressure constant and calculate the critical strain for a range of normalized wavelength ( $\bar{L}_{\rm c}=L/H_{\rm f}$ ) for various values of stiffness ratios  $\beta$  (Figs. 6 and 7). First, we consider the case where the pressure is  $P_{\rm 2}/\mu_{\rm f}=0.5$  (regions A and B in Fig. 4). In the soft-film regime (region A), the threshold strain values are the same for different stiffness ratios, meaning that the stability of the system does not depend on the stiffness ratio (Fig. 6a). However, in region B, the system becomes much more unstable as the film gets stiffer than the substrate (Fig. 6b).

Next, the same analysis is performed with a similar range of stiffness ratio, except for a pressure loading which is higher than the film's stiffness ( $P_2/\mu_{\rm f}=3.5$ , regions C and D in Fig. 4). The results show that the stiffness ratio strongly affects the stability of the bilayer in the cases of both soft and stiff films (Fig. 7). This is notable, as previous research on bilayers without surface pressure has indicated that instability properties are the same for all soft-film systems ( $\beta < 1$ ) [11]. We also note that the effect of stiffness is not monotonic, with the stability of the bilayer increasing as the stiffness ratio approaches one, and decreasing as the stiffness ratio increases or decreases from there.

#### 5.3.2. Influence of pressure on the stability

In the previous section, we considered two cases for the normalized pressure,  $P_2/\mu_{\rm f}=0.5$  and  $P_2/\mu_{\rm f}=3.5$ , and discussed the effect of soft and stiff films. Here we consider a broader range of normalized pressure values (Fig. 8). As seen in region A of Fig. 4, soft films with  $P_2/\mu_{\rm f}<2$  show no effect from the stiffness ratio. Instead, their buckling behavior is dominated by the effects of pressure (Fig. 8a); increasing the pressure decreases the stability of the bilayer significantly. As the film gets stiffer than the substrate (region B of Fig. 4), both increasing pressure and the stiffness ratio decrease the threshold critical strain values.

The buckling behavior of the bilayer under compression changes strikingly as the pressure increases,  $P_2/\mu_{\rm f} > 2$  (Fig. 4, region C and D), with an instantaneous increase in the threshold strains (Fig. 8b). This implies that an increase in normalized pressure temporarily increases the buckling stability of the system, while further increases in pressure make the system more unstable.

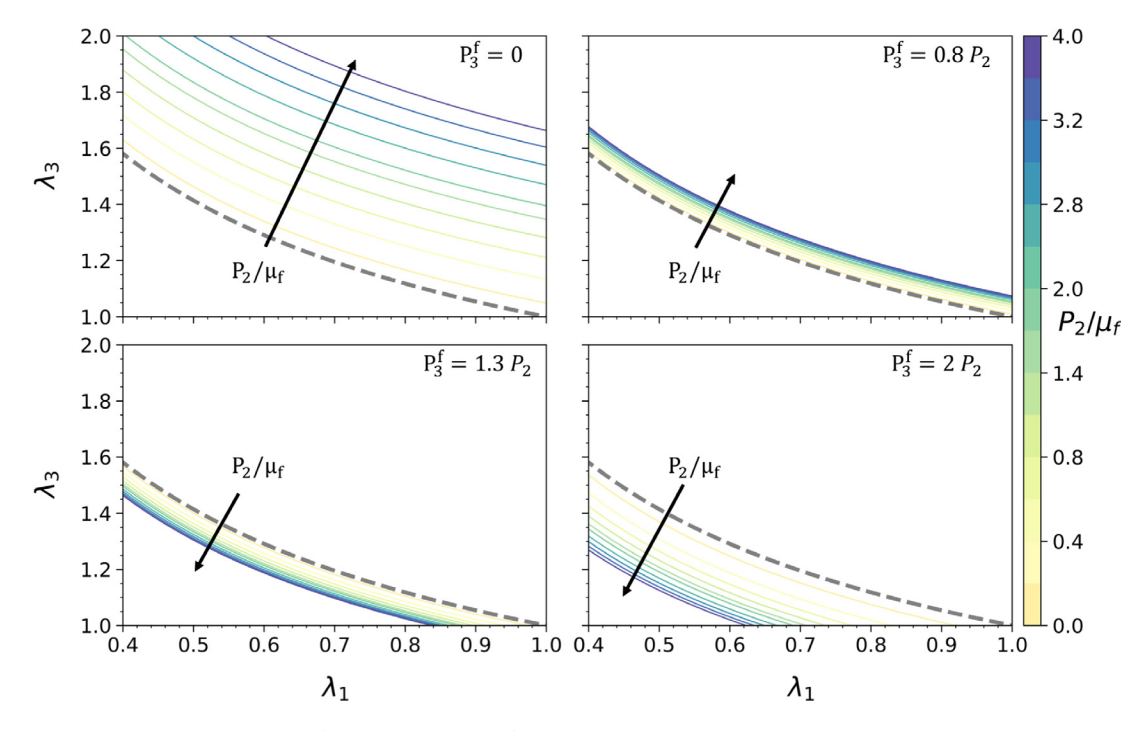


Fig. 3. Transverse stretch  $\lambda_3$  vs. axial stretch  $\lambda_1$ .  $P_2 < P_3^f$  in top row, and  $P_2 > P_3^f$  in bottom row. The gray-dashed line represents the result for a stress-free bilayer under uniaxial compression where  $\lambda_3 = 1/\sqrt{\lambda_1}$ .

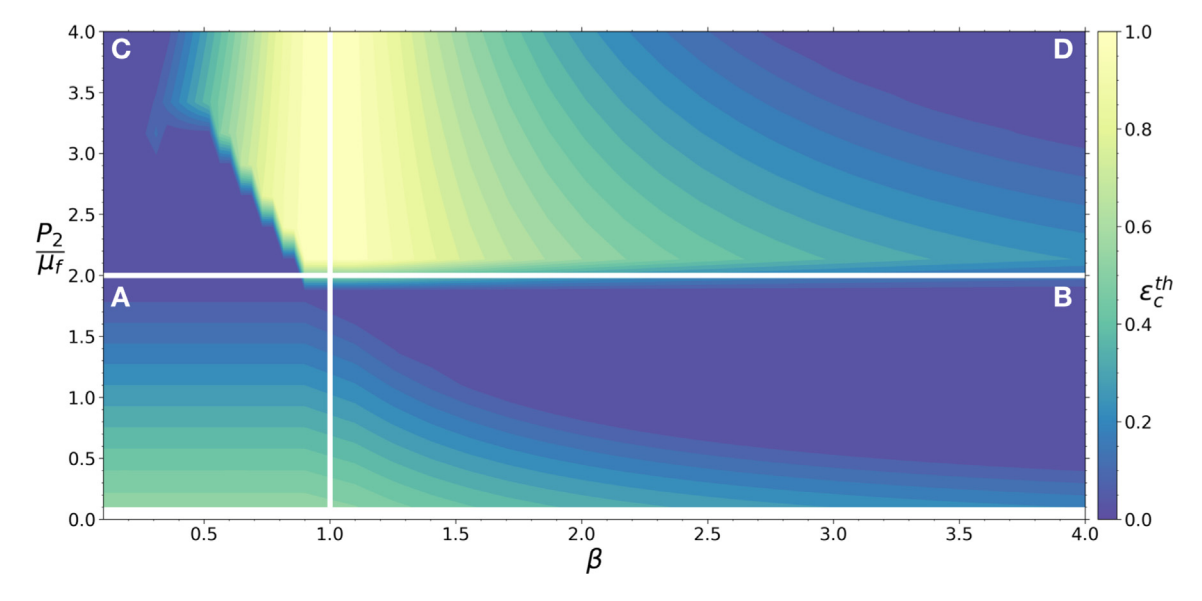


Fig. 4. Normalized pressure vs. stiffness ratio. The threshold critical strain is calculated for 1600 combinations of the normalized pressure and stiffness ratio, with  $P_3 = 1.3 P_2$ .

# 5.3.3. Discontinuous variation of threshold strains observed in soft film regime

The threshold strain diminishes to its minimum value continuously as pressure increases in both regions A and B. In Section 5.3.2, we discussed that a sudden increase in the threshold strains arises when  $P_2/\mu_{\rm f}$  becomes greater than 2. In region D, where the film is stiffer than the substrate, the buckling resistance of the bilayer increases when  $P_2/\mu_{\rm f} > 2$ , and it can be seen that the threshold strains suddenly jump from its minimum. This is because in this region, our analytical solution predicts that the system will approach, but not reach, an unstable point under low levels of compression ( $\lambda_1 \lesssim 1$ ). Instead, the unstable point is predicted to occur under low levels of tension ( $\lambda_1 \gtrsim 1$ ). Further investigation, including finite element and/or experimental approaches might be necessary to reveal the actual nature of the instability in this

region. This phenomenon does not occur precisely at  $P_2/\mu_{\rm f}=2$  in the regime of soft films (Fig. 4, region C), but rather at higher values of pressure. Also, in region C, we observe that as the stiffness of the film increases (the stiffness ratio approaches one), the bilayer system will endure higher amounts of pressure before buckling happens.

## 5.3.4. Regions of pressure-insensitivity

As the stiffness ratio increases, the threshold strain appears to approach an asymptotic value (Figs. 8a and 8b). When we expand the range of stiffness ratios to  $1 < \beta < 100$ , this becomes more clear. As the stiffness contrast of the system increases, it becomes very unstable, and the effect of applied pressure on the instability seems to vanish. This shows that the effect of pressure is only relevant for sufficiently low stiffness contrast,  $\beta \lesssim 10$  (Fig. 9). This is similar to the findings of our

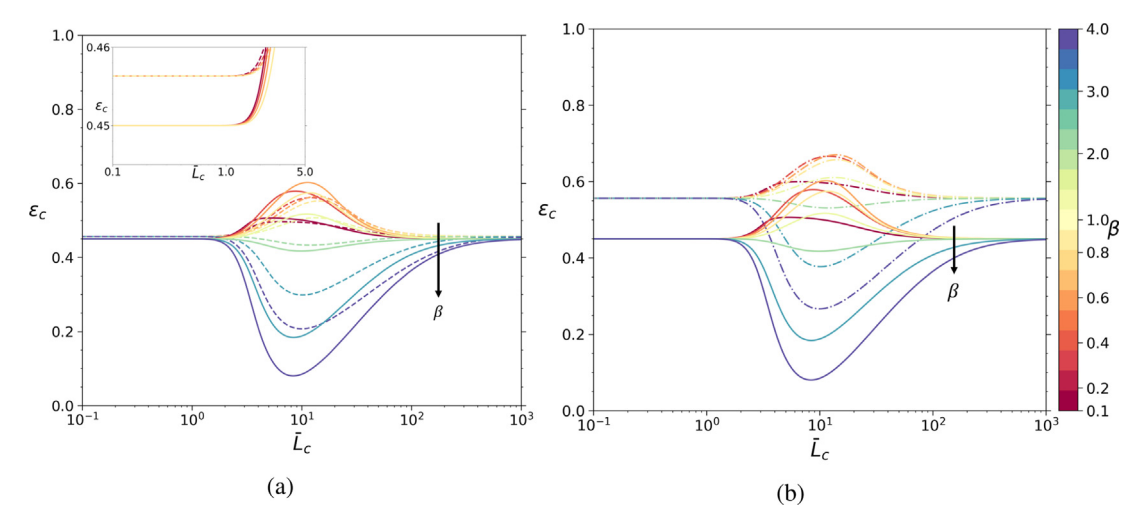


Fig. 5. Critical strain vs. normalized wavelength for eight different stiffness ratios, ranging from 0.1 (softer film) to 4 (stiffer film). Solid lines depict non-zero stress boundary conditions  $(P_2/\mu_{\rm f}=0.5,\ P_3=1.3P_2)$  of a cuboid bilayer under uniaxial compression, while dashed lines depict zero stress boundary conditions under (a) plane strain and (b) uniaxial compression [11]. The inset in (a) shows that the threshold critical values for  $\beta<1$  do differ, although only slightly, in the pressure and no-pressure case.

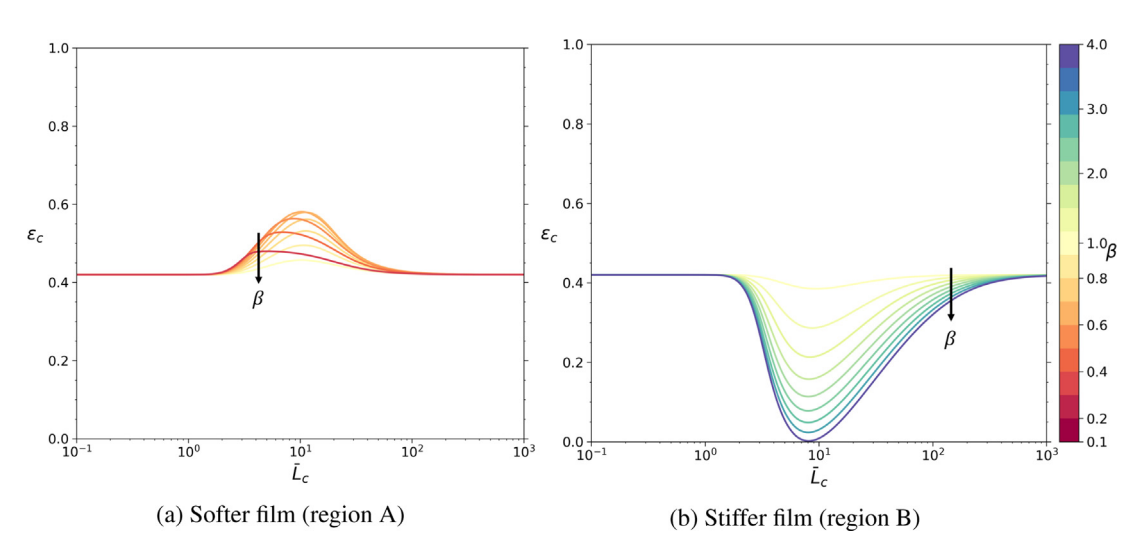


Fig. 6. Critical strain vs. critical wavelength for multiple stiffness ratios at  $P_2/\mu_{\rm f}=0.5,\ P_3=1.3P_2.$ 

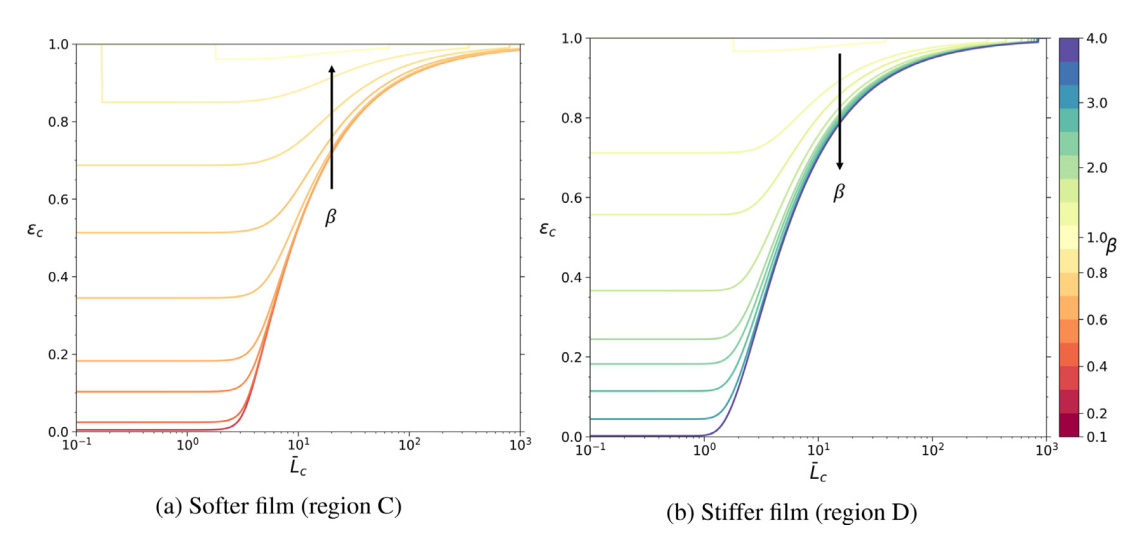


Fig. 7. Critical strain vs. critical wavelength for multiple stiffness ratios at  $P_2/\mu_{\rm f}=3.5,\ P_3=1.3P_2$ .

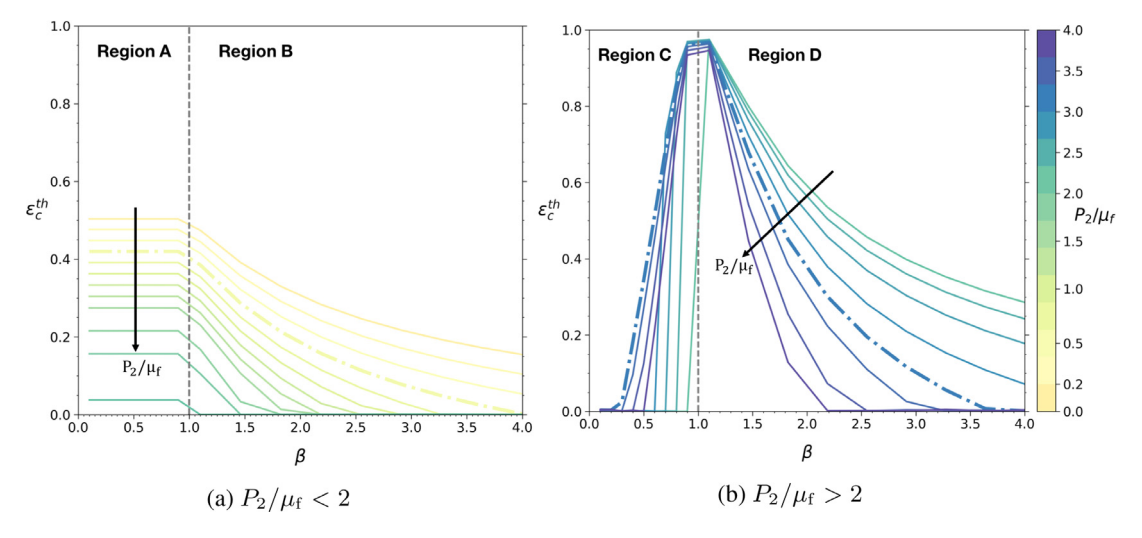


Fig. 8. Threshold critical strain vs. stiffness ratio for multiple normalized pressures. The dashed–dotted lines in (a) and (b) are the threshold strains of Figs. 6 (where  $P_2/\mu_{\rm f}=0.5$ ) and 7 (where  $P_2/\mu_{\rm f}=3.5$ ), respectively.

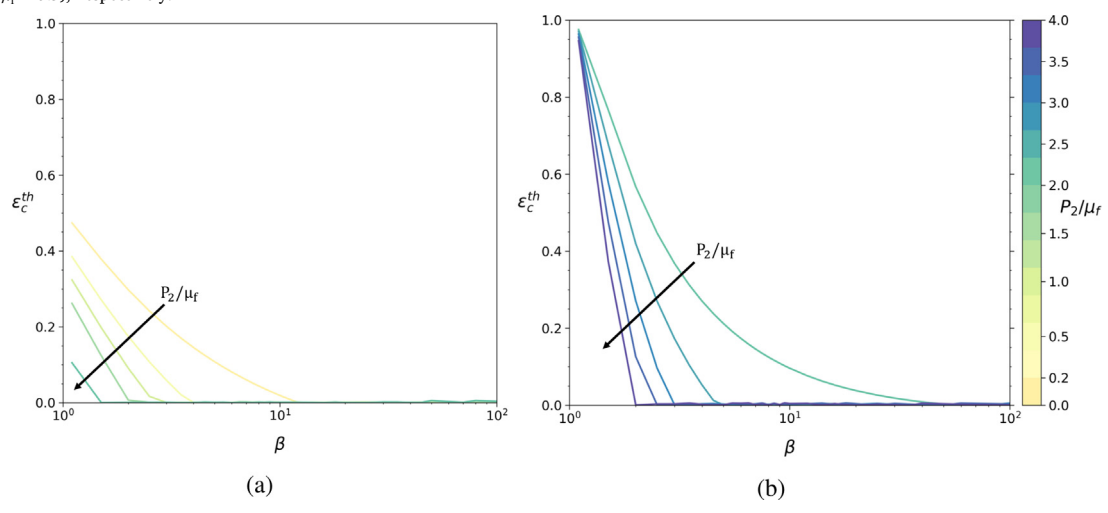


Fig. 9. Threshold strain values in stiff film regime under different normalized pressures  $P_2/\mu_{\rm f}$ , across a large range of stiffness ratios.

previous study that concluded that loading mode only affects stability when  $\beta \lesssim 10$  [11].

## 6. Conclusion

Although the effect of stiffness ratio in a bilayer system has been heavily studied, there has been little investigation into the effect of applied pressure on stability. In this study, we investigated the wrinkling response of an inhomogeneous bilayer structure, consisting of a dissimilar film and a substrate, under varying levels of applied surface pressure. We focused on bilayered materials with similar mechanical properties, as we intended to investigate the influence of the cerebrospinal fluid pressure on the instabilities of the brain tissue. We applied a variational method to minimize the free energy functional for the 3-D bilayer model and obtained the equations for the eigenvalue problem. Using a linear stability analysis of a film/substrate bilayer under compression, we showed that the pressure plays a role in the instability of the system. In a brief comparison, we show that the bilayer system under uniform compression with pressure applied to the top surface is always more unstable than the same system under uniaxial compression or plane strain compression. Our study indicates that when the film is softer than the substrate, the instability of the system generally does not depend on the stiffness ratio. On the other hand, the effects of pressure on the instability vanish when the ratio between

the stiffness of the film and substrate exceeds 10. Also, the pressure loses its influence when the stiffness ratio approaches one. Finally, we identified a discontinuity in threshold strains when the pressure is more than two times the film's stiffness, indicating an instant increase in the stability of the film/substrate bilayer. The results of this linearized stability study show the significance of surface pressure effects on the bilayer buckling behavior, and the need to account for these effects particularly in systems with sufficiently low stiffness contrast.

## CRediT authorship contribution statement

**Mohsen Darayi:** Methodology, Software, Writing - original draft, Visualization. **Maria A. Holland:** Conceptualization, Writing - review & editing, Supervision, Funding acquisition.

## **Declaration of competing interest**

The authors declare that they have no known competing financial interests or personal relationships that could have appeared to influence the work reported in this paper.

## Acknowledgments

This work was supported by the National Science Foundation, USA [IIS 1850102].

#### References

- M.A. Holland, K.E. Miller, E. Kuhl, Emerging brain morphologies from axonal elongation, Ann. Biomed. Eng. 43 (7) (2015) 1640–1653, http://dx.doi.org/10. 1007/s10439-015-1312-9.
- [2] M.J. Razavi, T. Zhang, X. Li, T. Liu, X. Wang, Role of mechanical factors in cortical folding development, Phys. Rev. E 92 (3) (2015) 032701, http: //dx.doi.org/10.1103/PhysRevE.92.032701.
- [3] J. Lee, S. Chung, H. Song, S. Kim, Y. Hong, Lateral-crack-free, buckled, inkjet-printed silver electrodes on highly pre-stretched elastomeric substrates, J. Phys. D 46 (10) (2013) 105305, http://dx.doi.org/10.1088/0022-3727/46/10/105305.
- [4] X. Wang, H. Hu, Y. Shen, X. Zhou, Z. Zheng, Stretchable conductors with ultrahigh tensile strain and stable metallic conductance enabled by prestrained polyelectrolyte nanoplatforms, Adv. Mater. 23 (27) (2011) 3090–3094, http: //dx.doi.org/10.1002/adma.201101120.
- [5] E. Guzman-Maldonado, P. Wang, N. Hamila, P. Boisse, Experimental and numerical analysis of wrinkling during forming of multi-layered textile composites, Compos. Struct. 208 (2019) 213–223, http://dx.doi.org/10.1016/j.compstruct. 2018 10 018
- [6] P. Hallander, M. Akermo, C. Mattei, M. Petersson, T. Nyman, An experimental study of mechanisms behind wrinkle development during forming of composite laminates, Compos. Part A 50 (2013) 54–64, http://dx.doi.org/10.1016/j. compositesa.2013.03.013.
- [7] M.A. Biot, Surface instability of rubber in compression, Appl. Sci. Res. Sect. A 12 (2) (1963) 168–182, http://dx.doi.org/10.1007/BF03184638.
- [8] J.M. Colin, M. Darayi, M.A. Holland, Stiffness contrast and separation influence wrinkling of adjacent layers in a homogeneous matrix, J. Appl. Mech. Trans. ASME 86 (4) (2019) 041004, http://dx.doi.org/10.1115/1.4042430.
- [9] C. Wang, S. Zhang, S. Nie, Y. Su, W. Chen, J. Song, Buckling of a stiff thin film on a bi-layer compliant substrate of finite thickness, Int. J. Solids Struct. 188–189 (2020) 133–140. http://dx.doi.org/10.1016/j.jisolstr.2019.10.012.
- [10] D.-H. Woo, Analysis of wrinkling behavior for anisotropic membrane, J. Korean Soc. Aeronaut. Space Sci. 33 (9) (2005) 48–55, http://dx.doi.org/10.5139/ JKSAS.2005.33.9.048.
- [11] M.A. Holland, B. Li, X.Q. Feng, E. Kuhl, Instabilities of soft films on compliant substrates, J. Mech. Phys. Solids 98 (2017) 350–365, http://dx.doi.org/10.1016/ j.jmps.2016.09.012.
- [12] L. Jin, A. Auguste, R.C. Hayward, Z. Suo, Bifurcation diagrams for the formation of wrinkles or creases in soft bilayers, J. Appl. Mech. Trans. ASME 82 (6) (2015) 061008, http://dx.doi.org/10.1115/1.4030384.
- [13] S. Nikravesh, D. Ryu, Y.L. Shen, Instabilities of thin films on a compliant substrate: Direct numerical simulations from surface wrinkling to global buckling, Sci. Rep. 10 (1) (2020) 1–19, http://dx.doi.org/10.1038/s41598-020-62600-z.
- [14] L. Zhuo, Y. Zhang, From period-doubling to folding in stiff film/soft substrate system: the role of substrate nonlinearity, Int. J. NonLinear Mech. 76 (2015) 1–7, http://dx.doi.org/10.1016/ji.ijnonlinmec.2015.05.002.
- [15] B. Li, C.Q. Zeng, S.F. Yin, X.Q. Feng, Regulating wrinkling patterns by periodic surface stiffness in film-substrate structures, Sci. China Technol. Sci. 62 (5) (2019) 747–754, http://dx.doi.org/10.1007/s11431-018-9390-3.
- [16] A. Javili, B. Dortdivanlioglu, E. Kuhl, C. Linder, Computational aspects of growth-induced instabilities through eigenvalue analysis, Comput. Mech. 56 (3) (2015) 405–420, http://dx.doi.org/10.1007/s00466-015-1178-6.
- [17] S. Budday, P. Steinmann, On the influence of inhomogeneous stiffness and growth on mechanical instabilities in the developing brain, Int. J. Solids Struct. 132–133 (2018) 31–41, http://dx.doi.org/10.1016/j.ijsolstr.2017.08.010.
- [18] Z. Zhao, J. Gu, Y. Zhao, Y. Guan, X.X. Zhu, Y. Zhang, Hydrogel thin film with swelling-induced wrinkling patterns for high-throughput generation of multicellular spheroids, Biomacromolecules 15 (9) (2014) 3306–3312, http:// dx.doi.org/10.1021/bm500722g.
- [19] P. Nardinocchi, E. Puntel, Swelling-induced wrinkling in layered gel beams, Proc. R. Soc. A 473 (2207) (2017) 20170454, http://dx.doi.org/10.1098/rspa.2017.
- [20] P. Sáez, A.M. Zöllner, Mechanics reveals the biological trigger in wrinkly fingers, Ann. Biomed. Eng. 45 (4) (2017) 1039–1047, http://dx.doi.org/10.1007/s10439-016-1764-6.
- [21] F. Xu, M. Potier-Ferry, Quantitative predictions of diverse wrinkling patterns in film/substrate systems, Sci. Rep. 7 (1) (2017) 1–10, http://dx.doi.org/10.1038/ s41598-017-18267-0.
- [22] Z.Y. Huang, W. Hong, Z. Suo, Nonlinear analyses of wrinkles in a film bonded to a compliant substrate, J. Mech. Phys. Solids 53 (9) (2005) 2101–2118, http://dx.doi.org/10.1016/j.jmps.2005.03.007.
- [23] R. Huang, Z. Suo, Instability of a compressed elastic film on a viscous layer, Int. J. Solids Struct. 39 (7) (2002) 1791–1802, http://dx.doi.org/10.1016/S0020-7683(02)00011-2.
- [24] S.H. Im, R. Huang, Wrinkle patterns of anisotropic crystal films on viscoelastic substrates, J. Mech. Phys. Solids 56 (12) (2008) 3315–3330, http://dx.doi.org/ 10.1016/j.jmps.2008.09.011.

- [25] M. Holland, S. Budday, A. Goriely, E. Kuhl, Symmetry breaking in wrinkling patterns: Gyri are universally thicker than sulci, Phys. Rev. Lett. 121 (22) (2018) 228002, http://dx.doi.org/10.1103/PhysRevLett.121.228002.
- [26] S. Budday, G. Sommer, C. Birkl, C. Langkammer, J. Haybaeck, J. Kohnert, M. Bauer, F. Paulsen, P. Steinmann, E. Kuhl, G.A. Holzapfel, Mechanical characterization of human brain tissue, Acta Biomater. 48 (2017) 319–340, http://dx.doi.org/10.1016/j.actbio.2016.10.036.
- [27] A. Rajesh, M. Kingston-hepner, D. Krishnakumar, Raised intracranial pressure, Paediatr. Child Health (U.K.) 27 (6) (2017) 260–267, http://dx.doi.org/10.1016/ i.paed.2017.01.016.
- [28] J. Hvedstrup, A. Radojicic, W. Moudrous, M.W. Herklots, A. Wert, M. Holzgraefe, M. Obermann, G.G. Schoonman, R.H. Jensen, H.W. Schytz, Intracranial pressure: A comparison of the noninvasive headsense monitor versus lumbar pressure measurement, World Neurosurg. 112 (2018) e576–e580, http://dx.doi.org/10.1016/j.wneu.2018.01.089.
- [29] V. Gafoor, B. Smita, J. Jose, Long-term response of cerebrospinal fluid pressure in patients with idiopathic intracranial hypertension - a prospective observational study, Ann. Indian Acad. Neurol. 20 (3) (2017) 220–224, http://dx.doi.org/10. 4103/aian.AIAN\_32\_17.
- [30] S.C.M. Lee, C.J. Lueck, Cerebrospinal fluid pressure in adults, J. Neuro-Ophthalmol. 34 (3) (2014) 278–283, http://dx.doi.org/10.1097/WNO. 0000000000000155.
- [31] J. Totafurno, M. Bjerknes, Morphogenesis and mechanical instability of a prestressed tissue, Biochem. Cell Biol. 73 (7–8) (1995) 565–574, http://dx.doi. org/10.1139/o95-062.
- [32] W. Yang, T.C. Fung, K.S. Chian, C.K. Chong, Instability of the two-layered thick-walled esophageal model under the external pressure and circular outer boundary condition, J. Biomech. 40 (3) (2007) 481–490, http://dx.doi.org/10. 1016/j.jbiomech.2006.02.020.
- [33] J. Shim, C. Perdigou, E.R. Chen, K. Bertoldi, P.M. Reis, Buckling-induced encapsulation of structured elastic shells under pressure, Proc. Natl. Acad. Sci. USA 109 (16) (2012) 5978–5983, http://dx.doi.org/10.1073/pnas.1115674109.
- [34] Y. Zhu, X.Y. Luo, H.M. Wang, R.W. Ogden, C. Berry, Three-dimensional non-linear buckling of thick-walled elastic tubes under pressure, Int. J. NonLinear Mech. 48 (2013) 1–14, http://dx.doi.org/10.1016/j.ijnonlinmec.2012.06.013.
- [35] D. Yang, B. Mosadegh, A. Ainla, B. Lee, F. Khashai, Z. Suo, K. Bertoldi, G.M. Whitesides, Buckling of elastomeric beams enables actuation of soft machines, Adv. Mater. 27 (41) (2015) 6323–6327, http://dx.doi.org/10.1002/ adma.201503188.
- [36] J. Marthelot, P.T. Brun, F.L. Jiménez, P.M. Reis, Reversible patterning of spherical shells through constrained buckling, Phys. Rev. Mater. 1 (2) (2017) 025601, http://dx.doi.org/10.1103/PhysRevMaterials.1.025601.
- [37] Y. Anani, G. Rahimi, On the stability of internally pressurized thick-walled spherical and cylindrical shells made of functionally graded incompressible hyperelastic material, Lat. Am. J. Solids Struct. 15 (4) (2018) e37, http://dx. doi.org/10.1590/1679-78254322.
- [38] N. Cheewaruangroj, K. Leonavicius, S. Srinivas, J.S. Biggins, Peristaltic elastic instability in an inflated cylindrical channel, Phys. Rev. Lett. 122 (6) (2019) 068003, http://dx.doi.org/10.1103/PhysRevLett.122.068003.
- [39] J. Sieber, J.W. Hutchinson, J.M.T. Thompson, Buckling thresholds for pre-loaded spherical shells subject to localized blasts, J. Appl. Mech. 87 (3) (2020) 031013, http://dx.doi.org/10.1115/1.4045588.
- [40] C. Zheng, X. Li, C. Mi, Reducing stress concentrations in unidirectionally tensioned thick-walled spheres through embedding a functionally graded reinforcement, Int. J. Mech. Sci. 152 (2019) 257–267, http://dx.doi.org/10.1016/j. ijmecsci.2018.12.055.
- [41] H. Alawiye, E. Kuhl, A. Goriely, Revisiting the wrinkling of elastic bilayersi: linear analysis, Philos. Trans. R. Soc. A 377 (2144) (2019) 20180076, http://dx.doi.org/10.1098/rsta.2018.0076.
- [42] H. Chen, L. Guo, J. Nie, T. Zhang, X. Hu, T. Liu, A dynamic skull model for simulation of cerebral cortex folding, in: Lect. Notes Comput. Sci. (Including Subser. Lect. Notes Artif. Intell. Lect. Notes Bioinformatics), in: LNCS, vol. 6362, Med Image Comput Comput Assist Interv, 2010, pp. 412–419, http://dx.doi.org/ 10.1007/978-3-642-15745-5 51.
- [43] R.W. Ogden, Non-Linear Elastic Deformations, Courier Corporation, 1997.
- [44] Y. Cao, J.W. Hutchinson, From wrinkles to creases in elastomers: the instability and imperfection-sensitivity of wrinkling, Proc. R. Soc. A 468 (2137) (2012) 94–115, http://dx.doi.org/10.1098/rspa.2011.0384.
- [45] J. Colin, M.A. Holland, Layer wrinkling in an inhomogeneous matrix, Int. J. Solids Struct. 156–157 (2019) 119–125, http://dx.doi.org/10.1016/j.ijsolstr. 2018.08.004.
- [46] C.J. Ridders, A new algorithm for computing a single root of a real continuous function, IEEE Trans. Circuits Syst. 26 (11) (1979) 979–980, http://dx.doi.org/ 10.1109/TCS.1979.1084580.